



# ***SEMIC*: An efficient surface energy and mass balance model applied to the Greenland ice sheet**

Mario Krapp<sup>1,2</sup>, Alexander Robinson<sup>3,1</sup>, and Andrey Ganopolski<sup>1</sup>

<sup>1</sup>Potsdam Institute for Climate Impact Research

<sup>2</sup>Department of Zoology, University of Cambridge

<sup>3</sup>Dpto. Astrofísica y CC de la Atmósfera, Universidad Complutense de Madrid

Correspondence to: mariokrapp@gmail.com

**Abstract.** We present *SEMIC*, a Surface Energy and Mass balance model of Intermediate Complexity for snow and ice covered surfaces such as the Greenland ice sheet. *SEMIC* is fast enough for glacial cycle applications, making it a suitable replacement for simpler methods such as the positive degree day method often used in ice sheet modelling. Our model explicitly calculates the main processes involved in the surface energy and mass balance, while maintaining a simple interface and minimal data input to drive it. In this novel approach, we parameterise diurnal temperature variations in order to more realistically capture the daily thaw-freeze cycles that characterise the ice sheet mass balance. We show how to derive optimal model parameters for *SEMIC* to reproduce surface characteristics and day-to-day variations similar to the regional climate model MAR (Modèle Atmosphérique Régional) and its incorporated multi-layer snowpack model. A validation test shows that *SEMIC* simulates future changes in surface temperature and surface mass balance in good agreement with the more sophisticated multi-layer snowpack model included in MAR. With this paper, we present a physically-based surface model to the ice sheet-modelling community that is computationally fast enough for long-term integrations, such as glacial cycles or future climate change scenarios.

## **1 Introduction**

Currently, surface melt accounts on average for about half of the observed Greenland ice sheet loss; the other half is lost through basal melt and ice discharge across the grounding line, i.e., calving (van den Broeke et al., 2009). Recent observations show that Greenland's surface mass balance is further declining (Hanna et al., 2013). The positive surface mass balance can no longer compensate losses via ice discharge and is therefore regarded as a dominant source of Greenland's total mass loss. The extreme melt season in 2012 exposed the Greenland ice sheet's vulnerability to long-lasting temperatures anomalies (Nghiem et al., 2012). As more marine terminating glaciers further retreat (Thomas et al., 2011), the partitioning of ice loss is likely to shift further towards the declining surface mass balance.

Numerical simulations of large land ice masses, such as the Greenland and the Antarctic ice sheets, require numerical models to be fast because the response time of ice sheets to changes in the surface mass balance is slow, on the order of years to tens of millennia (Cuffey and Paterson, 2010). Hence, many thousands of years of model integration are required to spin-up the model or to simulate one or several glacial cycles.



The simplest, fastest, and still most widely used method to estimate the surface mass balance of glaciers and ice sheets is the so-called positive-degree-day (PDD) approach (e.g. Reeh, 1991; Ohmura, 2001). It is based on the empirical relationship between surface melt rate and daily mean surface air temperature. Although PDD parameters are tuned to correctly represent present-day melting rates, past climates may require different parameter values. For instance, the PDD approach with its present-day parameter values is not applicable to orbitally-forced climate change (van de Berg et al., 2011; Robinson and Goelzer, 2014).

Here, we propose a physically-based model utilising an energy balance approach that is inherently consistent with a variety of climate states different from today, e.g., future warming, last glacial maximum, or the Eemian interglacial. Our proposed model not only accounts for temperature changes but also for changes in other climate factors, such as insolation, turbulent heat fluxes, and surface albedo.

The Surface Energy and Mass balance model of Intermediate Complexity (SEMIC) is based on a surface scheme that has already been used to study glacial cycles (Calov et al., 2005). SEMIC provides a process-based relationship between surface energy and surface mass balance changes. The approach described here guarantees a consistent treatment of melting and meltwater refreezing; both are important processes for the mass budget of ice sheets (Reijmer et al., 2012).

Compared to more sophisticated multi-layer snowpack models, which include snow metamorphism or vertical temperature profile calculations, SEMIC has a reduced complexity, one-layer snowpack. This saves computation time and allows for integrations on multi-millennial time scales. SEMIC calculates the daily surface energy and mass balance throughout the year but is also fast enough to focus on longer time scales when climatological changes determine the trend of the surface energy and mass balance.

Numerical ice sheet models need the annual mean surface temperatures and annual mean surface mass balance of ice as boundary conditions at the surface. Both are calculated by SEMIC, which can thus be directly coupled to the ice sheet model. There is a multitude of possible applications for SEMIC, for example, under projections of future warming for the next centuries or glacial cycle simulations. In this paper, we will discuss the future warming projections of the RCP8.5 scenario (Moss et al., 2010) to demonstrate the capabilities of our model.

The paper is organised as follows. In the next section, we present the model equations and their parameters. In Sect. 3, we describe the calibration procedure used to constrain the free model parameters and we estimate the sensitivity of the calculated surface mass balance with respect to the model parameters. In Sect. 4, we validate our model against regional climate model data for a future warming scenario. We discuss our findings in Sect. 5 and conclude in Sect. 6.

With this paper we acknowledge, support, and encourage research that follows standards with respect to scientific reproducibility, transparency, and data availability. The model source code and the authors' manuscript source is freely available and accessible online.



## 2 Model Description

SEMIC is based on the calculation of the mass and energy balance of the snow and/or ice surface. We assume that the surface temperature  $T_s$  responds to changes in the surface energy balance according to

$$c_{\text{eff}} \frac{dT_s}{dt} = (1 - \alpha)SW^\downarrow + LW^\downarrow - LW^\uparrow - H_S - H_L - Q_{M/R} \quad (1)$$

- 5 where  $\alpha$  is the surface albedo,  $SW^\downarrow$  is the downwelling shortwave radiation,  $LW^\downarrow$  is the downwelling longwave radiation,  $LW^\uparrow$  is the upwelling longwave radiation,  $H_S$  and  $H_L$  are the sensible and latent heat flux to the atmosphere, and  $Q_{M/R}$  is the residual heat flux available for melting or refreezing of snow and ice. The parameter  $c_{\text{eff}}$  denotes the effective heat capacity of the snowpack. In a strict sense of the term “energy balance” the left-hand-side of Eq. (1) should be zero. Here, we assume that surface temperature and the energy are not in equilibrium because the snowpack or surface exerts some thermal inertia.
- 10 Temperatures of snow- and ice-covered surfaces cannot exceed  $0^\circ$  C. However, for computational purposes, we initially assume that  $T_s$  represents the potential temperature, which would be observed in the absence of phase transitions, i.e., melting or refreezing. Once, melting and refreezing has been computed (see Sect. 2.3), the residual heat flux  $Q_{M/R}$  in Eq. (1) keeps track of any heat flux surplus or deficit and is added back to the energy balance. This way,  $T_s$  never exceeds  $0^\circ$  C.

- For coupling to an ice sheet model, the surface mass balance for ice ( $SMB_i$ ) is computed by SEMIC. It separates the total  
 15 surface mass balance into the surface mass balance for snow and for ice:

$$SMB = SMB_s + SMB_i = P_s - SU - M + R, \quad (2)$$

$$SMB_s = P_s - SU - M_{\text{snow}} - C_{si}, \quad (3)$$

$$SMB_i = C_{si} - M_{\text{ice}} + R. \quad (4)$$

- Here,  $P_s$  is the snowfall rate and  $SU$  is the sublimation rate which is related to the latent heat flux via  $H_L/\rho_w L_s$ . The model  
 20 variable  $M$  is the total melting rate, i.e., the sum of snow and ice melt (denoted by the subscripts),  $R$  is the refreezing rate of liquid water (rain or melt water), and  $C_{si}$  is the compaction rate of snow which is turned into ice.

Changes in snowpack height  $h_s$  (in  $m$  water equivalent) are determined by the surface mass balance of snow:

$$\frac{dh_s}{dt} = SMB_s, \quad \text{with } h_s \in \max(0, h_{s,\text{max}}). \quad (5)$$

- If the snow height  $h_s$  exceeds a certain threshold  $h_{s,\text{max}}$  (here set to 5 m) snow is transformed into ice—in a simple way  
 25 resembling snow compaction:

$$\int_0^{\Delta t} C_{si} dt = \max(0, h_s - h_{s,\text{max}}). \quad (6)$$

The described equations are solved using an explicit time-step scheme. For faster computation we use a time step of one day. In principle, the use of monthly input data is also supported but would require interpolation to daily time steps.



## 2.1 Surface heat fluxes

We describe the outgoing longwave radiation as a function of surface temperature according to the Stefan–Boltzmann law:

$$LW^\uparrow = \sigma T_s^4. \quad (7)$$

For the turbulent heat exchange (sensible and latent) we use a standard bulk formulation

$$5 \quad H_S = C_S \rho_a c_{p,a} u_s (T_s - T_a) \quad (8a)$$

$$H_L = C_L \rho_a L_s u_s (q_s - q_a) \quad (8b)$$

with sensible and latent heat exchange coefficients  $C_S$  and  $C_L$ , air density  $\rho_a$ , specific heat capacity of air  $c_{p,a}$ , surface wind speed  $u_s$ , air temperature  $T_a$ , latent heat of sublimation/deposition  $L_s$ , and air specific humidity  $q_a$ . Specific humidity over the snow or ice surface ( $q_s$ ) is assumed to be saturated and depends on surface pressure  $p_s$  and saturation water vapour pressure  $e^*$

$$10 \quad q_s = \frac{e^* \epsilon}{e^* (\epsilon - 1) + p_s}, \quad \text{where} \quad (9)$$

$$e^* = 611.2 \exp\left(a \frac{T_s - T_0}{T_b + T_s - T_0}\right)$$

with  $\epsilon = 0.62197$ , the ratio of the molar weights of water vapour and dry air, and coefficients  $a$ ,  $T_b$ , which are prescribed for vapour pressure over water ( $a = 17.62$ ,  $T_b = 243.12$  K) or ice/snow ( $a = 22.46$ ,  $T_b = 272.62$  K).  $T_0$  denotes the freezing point of water, 273.15 K. See, Gill (1982) for details.

## 15 2.2 The diurnal cycle of thawing and freezing

Because we use daily time steps, processes on time scales shorter than one day cannot be resolved explicitly. Hence, we cannot explicitly account for the thawing during daytime and the freezing during nighttime which is quite usual for the melting season on Greenland. The absorbed shortwave radiation, for example, can exhibit large diurnal variations, especially when the surface albedo is low (Cuffey and Paterson, 2010). During the day, near surface temperatures may rise above freezing temperature and snow or ice starts to melt. During the night, temperatures drop below freezing and any liquid water such as previously melted water can refreeze within the snowpack.

To account for this process we introduce a parametrisation for the diurnal cycle of thawing and freezing. We simply assume a sinusoidal temperature curve  $T(t)$  throughout the day (here, units of time  $t$  are hours  $h$ ) around a given mean surface temperature  $T_s$  (here, we refer to  $T_s$  with units in °C) with amplitude  $A$ , i.e., a cosine function (Fig. 1):

$$25 \quad T(t) = T_s - A \cos\left(\frac{2\pi}{24}t\right) \quad (10)$$

For the sake of simplicity we use a single constant  $A$ , although in reality it is spatially and temporally dependent as shown in Fig. 1.

Melting and refreezing may then occur on the same day if (potential, not actual)  $T_s$  exceeds 0°C. The amount of melting and refreezing then depends on the amplitude  $A$  and the mean daily temperature  $T_s$  (Fig. 1). Fortunately, an analytical solution



to this problem exists. We calculate the roots of the cosine function and then integrate between the roots to solve for average above- and below-freezing mean surface temperatures  $T_s^+$  and  $T_s^-$ . The roots are

$$t_1 = \frac{24}{2\pi} \arccos\left(\frac{T_s}{A}\right), \quad t_2 = 24 - t_1.$$

Thus, the time span for temperatures above and below freezing is

$$5 \quad \Delta t_+ = t_2 - t_1 = 24 - 2t_1, \quad \text{and} \quad \Delta t_- = 2t_1.$$

This leads us to an expression for averages of above- and below-freezing temperatures  $T_s^+$  and  $T_s^-$ . These are the integrals of the cosine function

$$T_s^+ = \frac{1}{\Delta t_+} \int_{t_1}^{t_2} T(t) dt \quad (11a)$$

$$= \frac{24}{\pi \Delta t_+} \left[ -T_s \arccos\left(\frac{T_s}{A}\right) + A \sqrt{1 - \frac{T_s^2}{A^2}} + \pi T_s \right]$$

$$10 \quad T_s^- = \frac{1}{\Delta t_-} \int_0^{t_1} T(t) dt + \int_{t_2}^{24} T(t) dt \quad (11b)$$

$$= \frac{24}{\pi \Delta t_-} \left[ T_s \arccos\left(\frac{T_s}{A}\right) - A \sqrt{1 - \frac{T_s^2}{A^2}} \right].$$

This parameterisation depends on on the prescribed diurnal cycle amplitude,  $A$ , which affects the amount of melting and refreezing and, thus, the surface mass balance. Note, melt energy  $Q_m$  and “cold content”  $Q_c$  in the following Eq. (12) are calculated by using  $T_s^+$  and  $T_s^-$ , respectively. Without this parametrisation or with  $A$  set to zero melting and refreezing cannot occur at the same time step and instead, the actual surface temperature  $T_s$  must be used.

### 2.3 Melting and refreezing

Additional processes that affect the snowpack temperature are melting and refreezing. During 24 h the energy available for melt  $Q_m$  and refreezing (the so-called “cold content”)  $Q_c$  are defined as

$$20 \quad Q_m = \begin{cases} (T_s^+ - T_0) \frac{C_{\text{eff}}}{\Delta t} & \text{if } T_s^+ > T_0, \\ 0 & \text{if } T_s^+ \leq T_0, \end{cases} \quad (12a)$$

and

$$Q_c = \begin{cases} 0 & \text{if } T_s^- \geq T_0, \\ (T_0 - T_s^-) \frac{C_{\text{eff}}}{\Delta t} & \text{if } T_s^- < T_0. \end{cases} \quad (12b)$$



Thus, the potential melt is

$$M_{\text{pot}} = \frac{Q_m}{\rho_w L_m} \quad (13)$$

with water density  $\rho_w$ , latent heat of melting (or fusion)  $L_m$ , and time step  $\Delta t$ . Actual melt depends on how much solid water, i.e., snow or ice, is available for melt. If potential melt is larger than the current snow height all snow melts down and the excess melt energy is used to melt the underlying ice. Ice-free land is treated differently and the excess melt energy is used to warm the surface. The actual melt  $M$  is then the sum of melted snow and melted ice

$$M_{\text{snow}} = \min(M_{\text{pot}}, h_s / \Delta t) \quad (14a)$$

$$M_{\text{ice}} = M_{\text{pot}} - M_{\text{snow}} \quad (14b)$$

$$M = M_{\text{snow}} + M_{\text{ice}} \quad (14c)$$

The refreezing rate depends on the potential liquid water to be refrozen, i.e., the actual melt rate  $M$  and rainfall  $P_r$ . Analogous to the melt rates, the potential refreezing is given by

$$R_{\text{pot}} = \frac{Q_c}{\rho_w L_m}. \quad (15)$$

Suppose some liquid water, i.e., rain or melt water, exists within the snow pack. The “cold content”  $Q_c$  is then used to (virtually) turn liquid water into frozen water, i.e., snow or ice. We distinguish between refrozen rain and refrozen melt water

$$R_{\text{pot,rain}} = \min(R_{\text{pot}}, P_r) \quad (16a)$$

$$R_{\text{pot,melt}} = \min(\max(R_{\text{pot}} - R_{\text{pot,rain}}, 0), M_{\text{snow}}) \quad (16b)$$

$$R = R_{\text{rain}} + R_{\text{melt}} = R_{\text{pot,rain}} + R_{\text{pot,melt}}. \quad (16c)$$

We neglect refreezing of melted ice and treat ice melt as runoff.

As noted in the beginning of this section, melting consumes internal energy of the snowpack, while refreezing releases internal energy. SEMIC accounts for both melting and refreezing, and therefore the associated temperature change in Eq. (1) via  $Q_{M/R}$ —the residual energy for refreezing or melting.

$$Q_{M/R} = \rho_w L_m (M - R) \quad (17)$$

Here, we see how tightly the mass balance and the energy balance are coupled and that great care must be taken when the underlying surface processes are incorporated into one model.

## 2.4 Snow albedo parametrisation

We use a modified version of an albedo parametrisation for snow that depends on snow temperature (Slater et al., 1998). The original version describes albedos for the near-infrared and the visible band. Because the dependence on temperature of both albedo terms are similar, we combined these two into one albedo term.



The reasoning of a temperature-dependent snow albedo is as follows: Albedo declines if snow starts to melt and melting is much more likely for higher temperatures. The snow albedo above a certain temperature threshold, here  $T_{min}$ , is temperature dependent and starts to decline to the albedo of old snow, i.e.,  $\alpha_{s,min}$  as temperatures approach the melting point  $T_0$ . Below the temperature threshold  $T_{min}$ , we assume that snow does not change and has an albedo of fresh snow, i.e.  $\alpha_{s,max}$ . The relationship between snow albedo and temperature can, therefore, be described according to

$$\alpha_s = \alpha_{s,max} - (\alpha_{s,max} - \alpha_{s,min})t_m^3 \quad \text{with} \quad (18a)$$

$$t_m = \begin{cases} 0 & \text{if } T_s < T_0, \\ \frac{T_s - T_{min}}{T_0 - T_{min}} & \text{if } T_{min} \leq T_s < T_0, \\ 1 & \text{if } T_s > T_0. \end{cases} \quad (18b)$$

$T_{min}$  is set to 263.15 K as originally proposed (Slater et al., 1998).

The actual surface albedo  $\alpha$  is then the average of snow albedo  $\alpha_s$  and the prescribed background albedo  $\alpha_i$  for ice-covered or  $\alpha_l$  for ice-free land and depends on the critical snow height  $h_{crit}$

$$\alpha = \alpha_s - f_a(\alpha_s - \alpha_{bg}) \quad \text{where} \quad \alpha_{bg} = \begin{cases} \alpha_i & \text{for ice-covered or} \\ \alpha_l & \text{for ice-free land} \end{cases} \quad (19)$$

and  $f_a = \exp(-h_s/h_{crit})$ .

Although the snow albedo depends on temperature only, the grid-averaged albedo includes snow height as well as the characteristics of the underlying surface (i.e., ice or bare land), thus providing enough degrees of freedom to capture the variety of surface conditions over ice- and snow-covered regions.

## 2.5 Boundary conditions, initial conditions, and model performance

To drive the model we need as input: incoming short- and longwave radiation, near-surface air temperature, surface wind speed, near-surface specific humidity, surface pressure, snowfall, and rainfall either computed by an atmosphere model or prescribed as atmospheric forcing. For example, these fields can also be obtained from an interactive coupling to an atmospheric model. In order to evaluate the model, we choose to run the model offline using prescribed atmospheric forcing. Forcing fields are listed in Table 3.

In this paper, we use daily mean data from the regional climate model MAR, version 2 (Fettweis et al., 2013) to tune and optimise our model parameters. At its lateral boundaries MAR is forced by the general circulation model CanESM2 under historical conditions and under the global warming scenario RCP 8.5 (for details, see Fettweis et al., 2013). As input to SEMIC, we use the output of the last three model years of the 21st century scenario, i.e., 2098-2100, because they are representative of more extreme climatic conditions for the Greenland ice sheet. First, its associated surface mass balance exhibits the strongest seasonal variability at the end of the 21st century in RCP 8.5. And second, because those three years also capture substantial year-to-year variability. The model requires several years of spinup—especially the snow pack height  $h_s$  and



hence the associated surface albedo  $\alpha$  (see Eq. 19) responds rather slowly. We refrain to use more than three years because of the expected larger computational overhead<sup>1</sup>, which likely increases the overall computation time given that several thousands of calibration iterations are to be expected. Therefore, we loop 20 times over those three years to advance the variables from their initial conditions. The last iteration over the three years is then used for the comparison with MAR output.

5 On a modern laptop (e.g., MacBook Pro with an Intel Core i7, 2.8 GHz), 100 years of integration with daily time steps on a grid with 6,720 points (i.e., the MAR grid with 25 km horizontal resolution) take about 40 seconds. Of course, in coupled and stand-alone applications there is overhead for exchanging the variables and writing the output, thus, adding to the overall computation time. However, SEMIC is a fast model and therefore well suited for multi-millennial integration such as glacial cycles.

### 10 3 Model parameter calibration

To calibrate our free model parameters we minimise errors with respect to MAR output. Afterwards the optimised parameters are used to compare SEMIC with results for the whole historical period from 1970–2005 and for the warming scenario RCP 8.5 from 2006–2100.

At the model initialisation,  $T_s$  and  $\alpha_s$  are prescribed with values from MAR output of the first day, i.e., Jan 1 2098 and we  
15 set  $h_s = 1$  m. After a few time steps the fast responding variables  $T_s$  and  $\alpha_s$  are close their expected trajectories. However, response time for  $h_s$  is much longer and difficult to quantify because it depends on the slowly varying and highly sensitive mass balance terms. Therefore, several years of integration can be necessary for the model spinup. To account for the longer response time of  $h_s$  we loop 20 times over the three years, 2098–2100, creating an effective integration period of 60 years. From those 20 loops, the last iteration, i.e., the last loop, is used to estimate the error between SEMIC and MAR. The model  
20 initialisation and spinup is done every time SEMIC uses a new model parameter set, in order to treat each of those parameter settings in a comparable way.

The quality of our parameters is measured with the normalised centred root mean square error  $E$ . It is a good way to estimate how closely a test field (SEMIC output in our case) resembles a reference field (MAR output) in terms of correlation and variance (Taylor, 2001) while also allowing to assess variables with different units:

$$25 \quad E = \sqrt{\frac{1}{N} \sum_{n=1}^N \left[ \frac{(X_n - \bar{X}) - (Y_n - \bar{Y})}{\sigma_Y} \right]^2 + [\sigma_X / \sigma_Y - 1]^2} \quad (20)$$

Here,  $X$  is some SEMIC time series with  $N$  time steps. This could be any model variable, for example, averaged surface temperature  $T_s$ , net shortwave radiation  $SW_{net} = (1 - \alpha)SW^\downarrow$ , or surface mass balance  $SMB = P_s - SU - M + R$ . The symbol  $Y$  represents the corresponding MAR time series and the  $\sigma$ 's are the standard deviations of the time series. Overbars denote temporal averages of the time series.

<sup>1</sup>Three years of MAR data amounts already to 3.7Gb.



### 3.1 Minimising the cost function

To include Greenland’s diverse climate zones, we choose the time series (i.e., the  $X_n$ ’s and  $Y_n$ ’s) as being spatial averages over ice-free land and over three different ice-covered regions, all shown in Fig. 2. The three ice-covered regions crudely represent the main ablation zones at the ice-sheet margins (region 1), the main accumulation zone at ice-sheet interior (region 3), and a  
 5 mixed zone in between the main accumulation and ablation zones (region 2). We therefore calculate four different  $E$  values, one over ice-free land ( $E_L$ ) and three over the different ice-covered regions ( $E_{b1}, E_{b2}, E_{b3}$ ).

For our cost function we regard the following variables as important for the surface energy and mass balance: surface temperature  $T_s$ , net shortwave radiation  $SW_{net}$ , cumulative melt  $M_{cum}$ , and cumulative surface mass balance  $SMB_{cum}$ . The magnitude of this vector then defines our cost function  $J$

$$10 \quad J = \left\| (E_{L,T_s}, E_{b1,T_s}, \dots, E_{L,SW_{net}}, \dots, E_{b3,SMB_{cum}})^T \right\| \quad (21)$$

which we want to minimise. Note that we assign different weights to each of the regions based on their area.

The cost function  $J$  is minimised with a method called *Particle Swarm Optimisation*, described below. Using these calibration steps, we derive these optimal parameters values:  $A = 3.1$  K,  $\alpha_{s,min} = 0.77$ ,  $\alpha_{s,max} = 0.80$ , and  $h_{crit} = 0.09$  m which are also listed in Table 1.

### 15 3.2 Particle Swarm Optimisation

Because of the high dimensionality of the parameter space, a random search for the optimal parameters would need a large sample size in the order of  $\mathcal{O}(10^{5-6})$ . One optimisation technique that overcomes the problem of large sample sizes is the so-called *Particle Swarm Optimisation* (PSO) (Poli et al., 2007). PSO is based on social interaction among particles of the ‘swarm’. Initially, each particle is placed randomly in the parameter space and has a random velocity. For all particles the  
 20 cost function  $J$  is calculated (Eq. (21)). This determines the “fitness” of each individual and of the swarm as a whole. Now, each particle updates its current position and velocity in the parameter space depending on its current and current-best fitness position, and also on the global best-fitness position, with some random perturbations. The next iteration starts after all particles have moved. Eventually, the swarm as a whole moves to the minimum of the cost function  $J$ . For our parameter calibration we let 30 particles freely swarm within the four-dimensional parameter space. The global best-fitness solution found within 100  
 25 iterations<sup>2</sup> is then regarded as optimal.

### 3.3 Calibration results

The ice-sheet surface temperature is very well constrained by the atmospheric forcing fields. Therefore, the surface temperature in SEMIC is similar to the one calculated by MAR, as the annual mean differences and the ice-sheet averaged time series show (Fig. 3 and 5). The annual mean difference between SEMIC and MAR is about -0.2 K over the ice sheet and -0.2 K over ice-free

<sup>2</sup>Note, 100 iterations are a pre-defined upper limit and usually solutions tend to converge earlier.



land. While large parts of the ice sheet are slightly colder in SEMIC, temperatures at the ice divides are slightly warmer in SEMIC (see Fig. 3).

The surface mass balance is also well captured by SEMIC. The largest differences occur in the ablation zones of region 1 and 2 around the margin of the ice sheet. While melting over the northern part of the ice sheet is overestimated by SEMIC, it is underestimated over the southern part of the ice sheet. Nonetheless, the overall surface mass balance difference over the ice sheet between SEMIC and MAR is 0.13 mm/day, with SEMIC having an average surface mass balance of -1.38 mm/day (-1.51 mm/day in MAR). The relative difference between SEMIC and MAR is about 9% over the whole ice-sheet.

In regions where surface mass balance is positive, errors are small because accumulation is mainly prescribed by snowfall and to a lesser extent by sublimation/evaporation. Therefore, differences in ablation are more important because they arise dynamically from SEMIC. The introduced diurnal cycle parameterisation is critical here; it allows melting and refreezing within one time step which would be prohibited otherwise.

SEMIC produces less melt than MAR by 0.11 mm per day, with an average annual ice-sheet melt rate of 3.38 mm per day, which corresponds to a relative difference of about 5% compared to MAR. This is a result of more refreezing and larger sublimation rates in the ablation zone of the ice sheet.

SEMIC is able to capture both, the increase and decrease of surface mass balance as well as the seasonal melting as shown for the different regions in Fig. 4. As can be seen from Fig. 4, errors in melt rates and the surface mass balance accumulate over time. Particularly, over land and around the ice sheet margin (region 1 and partly region 2), the surface mass balance is slightly too large. This will have an effect on SEMIC's performance for the historical simulation and for RCP 8.5 (2005–2100).

The Taylor diagram in Fig. 7 summarises the performance of SEMIC compared to MAR and its multi-layer snowpack model. Except the surface mass balance in the interior of the Greenland ice sheet (region 3), all variables are reasonably close to the reference value of each regions' time series in terms of their variability, measured via their standard deviation and their match to the corresponding MAR variables, via their correlation. A detailed look into each time series (Fig.5) further supports our results that SEMIC and MAR variables are reasonably close to each other, especially during the whole melt season.

We find that the overall differences between SEMIC and MAR temperature and surface mass balance are reasonably small. SEMIC's annual mean values of surface temperature and surface mass balance are well suited for applications of interactive ice sheet models. The optimisation guarantees that the regionally averaged MAR and SEMIC time series are as close as possible (as defined by the cost function). Still, SEMIC is sensitive to the choice of parameters. Next we show how perturbed parameters around their optimal values affect the surface energy and mass balance of the ice sheet.

### 3.4 Parameter Sensitivity

We identified parameters that dominate model uncertainties and tested the parameter sensitivity on the model performance (e.g., Fitzgerald et al., 2012). We addressed the sensitivity of each SEMIC parameter listed in Table 1 (Fig. 6). Therefore, we varied each parameter freely while keeping the others at their optimal value. In this way, we estimated the contribution of each individual parameter on the cost function  $J$ . The effect of parameter variations on the individual cost function for surface



temperature  $T_s$ , surface mass balance  $SMB$ , surface melt, shortwave radiation  $SW_{net}$  is also calculated because each variable responds differently to different model parameters.

As can be seen for all parameter sensitivity graphs in Fig. 6, the Particle Swarm Optimisation was able to find the optimal value for each parameter, i.e., PSO minimises  $J$ . Therefore, we are confident that this optimal parameters set provides us with a globally optimised model setup.

The sensitivity to the diurnal cycle amplitude  $A$  is largest for melting because  $A$  directly defines the magnitude of daily melt rates. If  $A$  is too low, melt would be underestimated in SEMIC compared to MAR; and vice versa for too large  $A$ . However, the surface mass balance itself is less sensitive  $A$  than melting. The reason is that even if melting would be enhanced or suppressed, refreezing would almost compensate for that because it depends on the available meltwater.

The sensitivity to the maximum snow albedo  $\alpha_{s,max}$  is, as to be expected, largest for the net shortwave radiation because it directly limits the amount of radiation absorbed in the snowpack. Melting is also sensitive to the amount of shortwave radiation entering the snowpack. If more energy is available to raise the snowpack temperature the likelihood for melting is of course larger as well. Melt is also sensitive to changes in the minimum snow albedo  $\alpha_{s,min}$  but the surface mass balance exhibits an extraordinarily larger sensitivity.

Almost all cost functions show a sensitivity to variations of critical snow height  $h_{crit}$ . As before, the surface mass balance shows the largest sensitivity to changes in  $h_{crit}$ . Because  $h_{crit}$  determines how much weight we put on the snow albedo or the background albedo, i.e., bare ice or land albedo, it directly influences how much shortwave radiation is absorbed.

The parameter sensitivities reveal that our previously calibrated parameters are close to the calculated local minima for each of the individual cost functions.

## 4 Model validation

As a final step of the full model analysis, we use the optimised model parameters for the following two model validation runs: a) A historical run from 1970–2005 and b) an RCP8.5 scenario run from 2006–2100<sup>3</sup>. This time, we compare SEMIC with MAR for a whole time series instead of just a few years as done for the calibration. We take a closer look into the regional differences of surface temperature, surface melt, and surface mass balance over the four previously defined regions and calculate the corresponding time series of their annual mean values, as shown in Fig. 8.

Annual mean surface temperatures correspond well with MAR results and both time series are hard to distinguish from each other. To a lesser extent but still reasonably well, surface melt and surface mass balance are captured by SEMIC. The decline of surface mass balance throughout the 21st century in the RCP8.5 scenario is evident over the three ice-sheet regions, while the mass balance remains close to zero over ice-free land. Furthermore, SEMIC captures the year-to-year variations throughout the historical and the RCP8.5 period. This tells us that the newly introduced diurnal cycle parameterisation makes SEMIC more realistic and thus comparable to more comprehensive and complex multi-layer snowpack models. We believe

<sup>3</sup>Data is available at <ftp://ftp.climato.be/fettweis/MARv2/>



that a representation of the diurnal thawing and freezing cycle is essential for SEMIC and for physically correct mass balance modelling in general, and thus represent an important advance.

The overall performance of SEMIC with respect to the more sophisticated regional climate model MAR is satisfactory, given its intended use for long time-scale simulations. In the validation test we show that SEMIC is able to capture long-term trends of the Greenland ice sheet under the RCP8.5 scenario, while also reproducing the interannual variability exhibited by MAR.

## 5 Discussion

The definition of a cost function for the model calibration is a non-trivial task. SEMIC computes several variables which, in principle, could all be included in the cost function. We choose to take into account, first, the net shortwave radiation which is determined by the albedo parametrisation and its parameters and which in turn determines surface temperatures. Second and third, the surface mass balance and the surface temperature are considered, in anticipation of the interactive coupling to an ice-sheet model. And fourth, melting to account for the newly introduced diurnal cycle parameterisation of thawing and freezing. Still, it is clear that the choice of the cost function and the variables considered is subjective.

In the model calibration and validation we weighted each of the regions on the area. The area of the ice-free land and region 1, for example, is nearly as large as either region 2 or 3. Consequently, the influence of the smaller regions—here, land and region 1—is much smaller than that of the larger ones, such as regions 2 or 3, despite region 1 being a major driver of surface melting.

For the calibration of model parameters, we explicitly chose the last three years, 2098–2100, of the RCP8.5 scenario because those years exhibit the largest year-to-year variability as well as the largest surface melt rates/lowest mass balance rates for the available period from 1970–2100 (see Fig. 8). Pushing SEMIC to its limits in terms of forcing it with the most extreme climate conditions on record, is good evidence that our model can also represent less extreme climate conditions, such as, for example, the historical period or other any other RCP scenario.

There are two main reasons why surface temperature is better represented in SEMIC than the surface mass balance: 1) Surface temperature is determined by the driving atmospheric processes, which in our case are prescribed by MAR atmospheric forcing. Therefore changes in the atmosphere are directly reflected at the surface in terms of energy balance. 2) Surface mass balance is harder to constrain because the processes within the snowpack are more complex. Mass can be added by the atmosphere via rain and snowfall, and mass can be removed via melting. Within the snowpack melted water can refreeze if the temperature allows that. Refreezing depends on the available liquid water, i.e., rain or melted ice/snow, and on the energy budget, i.e., the “cold content”. The multitude of feedbacks involved in the surface mass balance makes it far less constrained by external forcing variables than surface temperature.

We only describe the large-scale effects of changes in the snowpack and we omit a microscopic description of snow physics (e.g., Vionnet et al., 2012). SEMIC can therefore be thought of as a surrogate of a more complex multi-layer snowpack model. We have developed SEMIC as a coupler between interactive ice sheet models and EMICs (Earth-System Models of Intermediate Complexity) or coarse resolution GCMs (General Circulation Models). SEMIC realistically represents the energy



transfer between atmosphere and surface as radiation and turbulent mixing of heat and water vapour, thus providing a general solution to the surface energy balance that is applicable for different climates and time scales.

Ice-free land and ice-covered land are treated differently in SEMIC because of the different physical processes involved. For example, the surface temperature of ice- and snow-free land has no upper limit as is the case for surface temperatures of ice, which is always lower than or equal to the freezing point. Generally, land albedo is much more variable than as described by the single bare land albedo used in SEMIC. Different land and vegetation types have different effects on the radiation budget. Consequently, net shortwave radiation errors in SEMIC are larger over ice-free land than over the ice sheet (Fig. 3).

Details in model representation also reveal differences between SEMIC and MAR. However, these differences are not so much related to the underlying physical principles, i.e., the assumption of energy and mass balance of the snow- and ice-covered surface, as to the choice of parameters made in order to match SEMIC variables to MAR variables.

SEMIC makes use of two simple but effective parameterisations that are important for its good performance: One is the surface albedo for which we already discussed the problem of the net shortwave radiation budget over ice-free land. Although the net shortwave radiation has an effect on the surface energy balance, errors do not translate directly into errors in the surface temperature (Fig. 3). One reason is that the contribution of sensible and latent heat flux is larger over ice-free land because of the larger temperature contrast. Latent heat flux, for example, is about 10 times larger over ice-free land than over the ice sheet.

Another reason for SEMIC's good performance is the diurnal cycle parametrisation, which allows for faster computation while adding the daily thaw–freeze cycle during melt season. The representation of the diurnal cycle of the whole ice sheet by a single constant value is somewhat problematic because in reality, it changes over time and location, depending on the climatic conditions, e.g., cloud cover and its effect on downwelling longwave radiation. Still, the overall results of SEMIC with respect to surface mass balance are satisfactory. The diurnal cycle opens many new aspects which could improve model results, e.g., a spatial dependence such as height-dependent amplitude or a direct calculation of the amplitude by the coupled atmospheric model, but this is beyond the scope of this paper. Also, a different or a more realistic albedo scheme could replace the current temperature-dependent implementation based on the work by Slater et al. (1998).

Our results underpin the consistent representation of the dominant processes involved in the complex interactions between snow- or ice-covered surfaces and the atmosphere. SEMIC incorporates simpler dynamics compared to multi-layer snowpack models, but represents the essential surface energy and mass balance processes, and is still fast in terms of computational time.

SEMIC is well suited for long-term integrations up to several millennia and has been successfully tested for the last 78,000 years (data taken from Heinemann et al., 2014, personal communication). From the 100 year run-time estimate we can assume that computation of the surface mass balance on every single day during one glacial cycle (of about 100 k years) would take about 11 h. Current state-of-the-art multi-layer snowpack models are not able to perform such long integrations but they also do not serve this purpose. Under these circumstances, using a much simpler model—such as SEMIC—is advised.

SEMIC is well suited for applications with global climate models which have just started to master glacial time scales (e.g., Heinemann et al., 2014). SEMIC will be part of the next version of the regional energy and moisture and balance model REMBO (Robinson et al., 2010) and is also ready to be coupled to an interactive ice-sheet model. SEMIC is considered as



an open-source project, therefore contributions are welcome, and we encourage and support the integration of SEMIC into ice-sheet models.

## 6 Conclusions

We have presented a new Surface Energy and Mass balance model of Intermediate Complexity (SEMIC) for snow- and ice-covered surfaces that is simple and fast enough for long-term integrations up to glacial time scales. SEMIC is a physically based model that accounts for energy and mass balance and it can be used as a surrogate for computationally intensive regional climate models with their multi-layer snowpack models. The most important features of SEMIC are a simple but effective surface albedo parameterisation and a parameterisation of the daily thaw-freeze cycle that allows partitioning between melting and refreezing. Compared to the more sophisticated regional climate model MAR, SEMIC represents surface temperature and surface mass balance considerably well. SEMIC matches climatological trends, e.g., the RCP8.5 warming scenario, while preserving realistic interannual variability. It incorporates a minimum number of free model parameters and a large effort was made to balance the complexity of the represented processes in favour of faster computation.

## 7 Scientific Reproducibility, Transparency, and Data Availability

We hereby acknowledge, support, and encourage research that follows standards with respect to scientific reproducibility, transparency, and data availability. Any model source code and the authors' manuscript source (typeset in  $\LaTeX$ ) is freely available and accessible online.

The project infrastructure covering individuals step starting from data download and preparation, model source code compilation, running the optimisation, running the calibrated model, running the model with historical and RCP8.5 scenario data, as well as the source code of this manuscript with its figures can be downloaded from the repository website <https://gitlab.pik-potsdam.de/krapp/semic-project>. See the project website's README.md for details. The project can also be cloned using git:

```
git clone -b v1.0 git@gitlab.pik-potsdam.de:krapp/semic-project.git
```

*Acknowledgements.* We would like to thank Xavier Fettweis for providing MAR/CanESM2 data. M.K. is also grateful to Malte Heinemann and Axel Timmermann for their kind hospitality during his research visit at the *International Pacific Research Center* (SOEST, University of Hawaii). A.R. was funded by the Marie Curie 7th Framework Programme (Project PIEF-GA-2012-331835, EURICE). M.K. was funded by the Deutsche Forschungsgemeinschaft (DFG) Project "Modeling the Greenland ice sheet response to climate change on different timescales".



symbol	range	value	description
$A$	0.0–5.0	<b>3.1</b>	amplitude of diurnal cycle (in K)
$\alpha_{s,\max}$	0.78–0.90	<b>0.80</b>	maximum snow albedo, i.e., fresh dry snow
$\alpha_{s,\min}$	0.60–0.78	<b>0.77</b>	minimum snow albedo, i.e., old or wet snow
$h_{\text{crit}}$	0.001–0.5	<b>0.09</b>	snow height for which the grid-average snow cover fraction is $1/e$ (in m)

**Table 1.** Model parameters with their initial range and their optimal value in bold face.

symbol	value	description
$\Delta t$	86,400 s	time step of one day
$c_{\text{eff}}$	$2 \cdot 10^6 \text{ J m}^{-3}$	effective heat capacity snow/ice (volumetric)
$C_S$	$2.0 \cdot 10^{-3}$	sensible heat exchange coefficient
$C_L$	$0.5 \cdot 10^{-3}$	latent heat exchange coefficient
$c_{p,a}$	$1000 \text{ J kg}^{-1} \text{ K}^{-1}$	specific heat capacity of air
$\sigma$	$5.67 \cdot 10^{-8} \text{ W m}^{-2} \text{ K}^{-4}$	Stefan–Boltzmann constant
$T_0$	273.15 K	freezing point of water
$\rho_w$	$1000 \text{ kg m}^{-3}$	density of liquid water
$L_s$	$2.83 \cdot 10^6 \text{ J kg}^{-1}$	latent heat of sublimation
$L_v$	$2.5 \cdot 10^6 \text{ J kg}^{-1}$	latent heat of vaporisation
$L_m$	$3.3 \cdot 10^5 \text{ J kg}^{-1}$	latent heat of melting ( $L_s - L_v$ )
$T_{\min}$	263.15 K	minimum temperature threshold for albedo parametrisation
$h_{s,\max}$	5.0 m	maximum snow height (cut-off)
$\alpha_i$	0.45	bare ice albedo, i.e., clean or blue ice
$\alpha_l$	0.15	bare land albedo

**Table 2.** Model constants and their description.



symbol	description
$SW^{\downarrow}$	downwelling shortwave radiation (in $\text{W m}^{-2}$ )
$LW^{\downarrow}$	downwelling longwave radiation (in $\text{W m}^{-2}$ )
$\rho_a$	air density (in $\text{kg m}^{-3}$ )
$u_s$	surface wind speed (in $\text{m s}^{-1}$ )
$T_a$	near-surface air temperature (in K)
$q_a$	near-surface specific humidity (in $\text{kg kg}^{-1}$ )
$p_s$	surface pressure (in Pa)
$P_s$	snowfall rate (in $\text{m s}^{-1}$ )
$P_r$	rainfall rate (in $\text{m s}^{-1}$ )

**Table 3.** Atmospheric forcing fields needed as input for this model.

		SEMIC	MAR	$\bar{\Delta}$	min $\Delta$	max $\Delta$
ice sheet	$T_s$ (in K)	255.6	255.4	-0.2	-0.7	2.7
	$SW_{net}$ (in $\text{W/m}^2$ )	30.6	31.3	-0.7	-9.6	7.7
	$SMB$ (in mm/day)	-1.38	-1.51	0.13	-3.15	5.12
	Melt (in mm/day)	3.38	3.57	-0.19	-4.66	2.94
land	$T_s$ (in K)	267.3	267.1	-0.2	-0.9	2.2
	$SW_{net}$ (in $\text{W/m}^2$ )	62.2	65.7	-3.5	-14.3	8.2
	$SMB$ (in mm/day)	0.15	-0.05	0.20	-0.09	1.20
	Melt (in mm/day)	1.38	1.27	0.11	-1.00	0.63

**Table 4.** Comparison of SEMIC and MAR. Shown are multi-year (2098–2100) mean averages over the ice sheet and ice-free land, their mean difference, and the minimum and maximum differences. Compare also to Fig. 3.

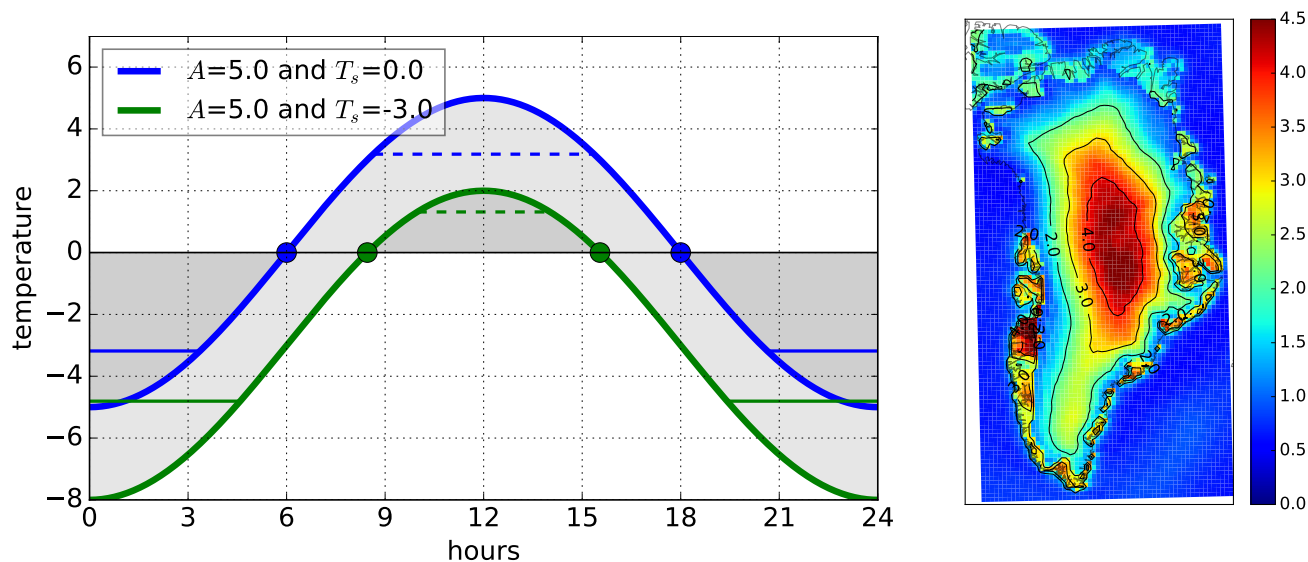


**Figure 1.** Left: The diurnal cycle parametrised as cosine function with amplitude  $A$  around the mean temperature  $T_s$ . The dashed horizontal line marks the analytical solution of the average above-mean temperature  $T_s^+$  and the solid horizontal lines mark the below-mean temperature  $T_s^-$  (see Eq. 11a and b). The circles denote the roots of the sinusoidal temperature cycle curve. Right: The mean diurnal cycle amplitude of air temperature for the summer season (JJA) in MAR for the years 2098–2100.

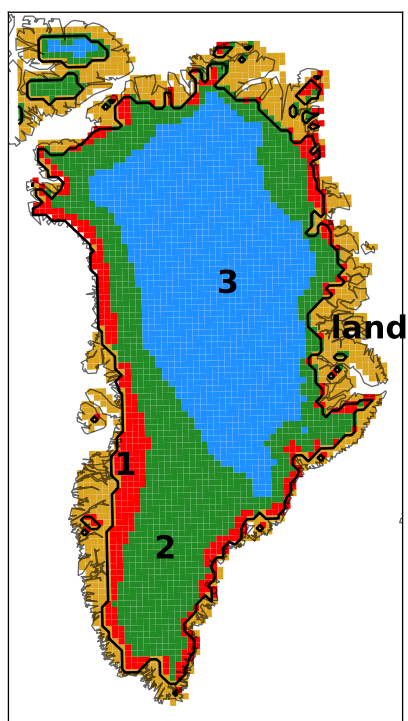


**Figure 2.** This region mask is used to estimate the region-averaged time series for the model calibration. Region 1 represents the ice margin, while the other regions represent areas with seasonal melt (2) or almost no melt (3). This mask is readily available from the MAR model data (named MSK).



### Multi-year Mean

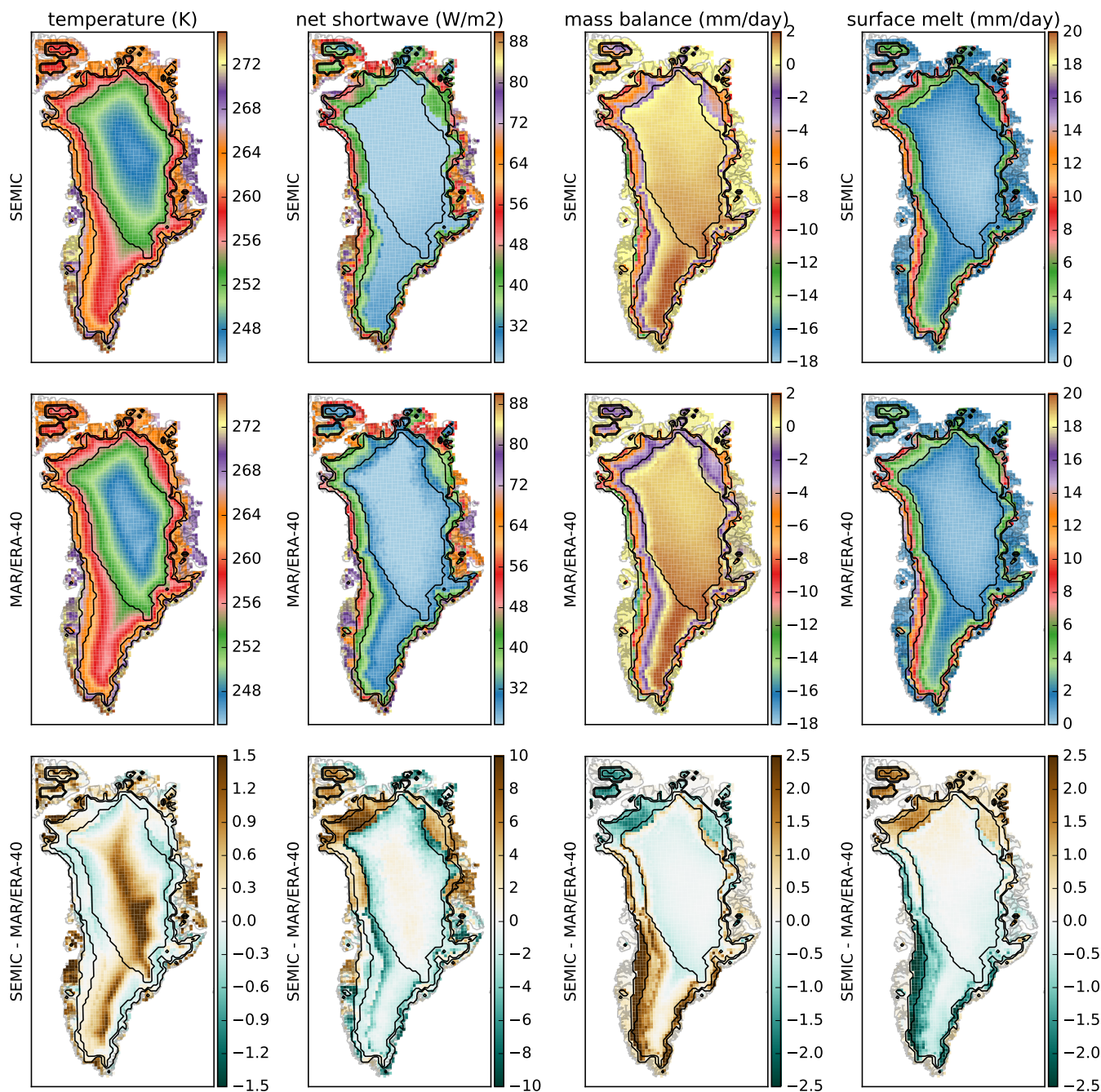


**Figure 3.** Comparison of modelled multi-year (2098–2100) mean surface temperature, net shortwave radiation, surface mass balance, as well as surface melt between SEMIC (after model optimisation) and MAR. Differences between SEMIC and MAR are depicted in the lower panels. The outlined contour shows the boundaries of the three ice-covered MAR regions as shown in Fig. 2. See Table 4 for values of minimum and maximum differences.

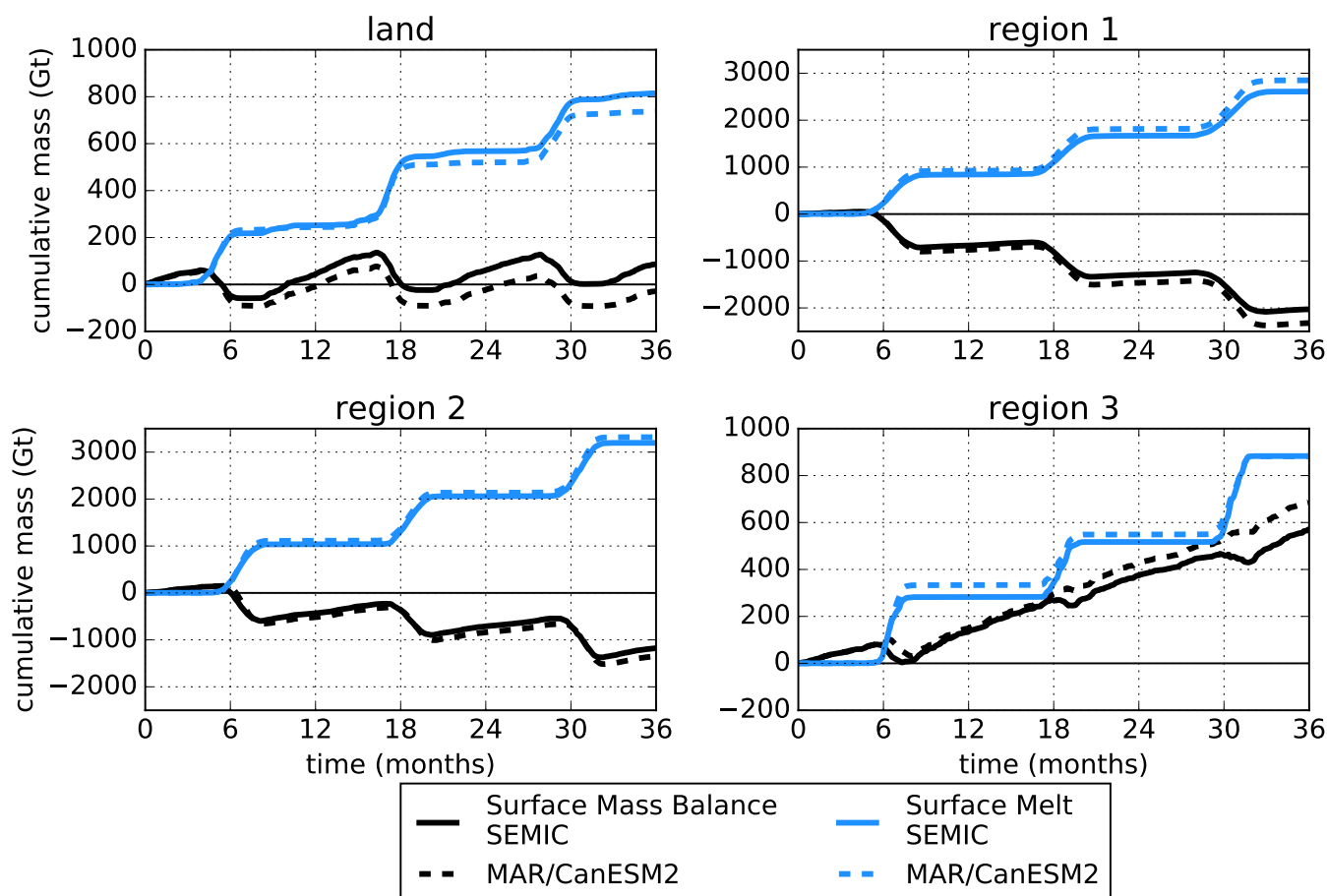


**Figure 4.** Cumulative sum of surface melt and surface mass balance over the four different regions as defined in Fig. 2.

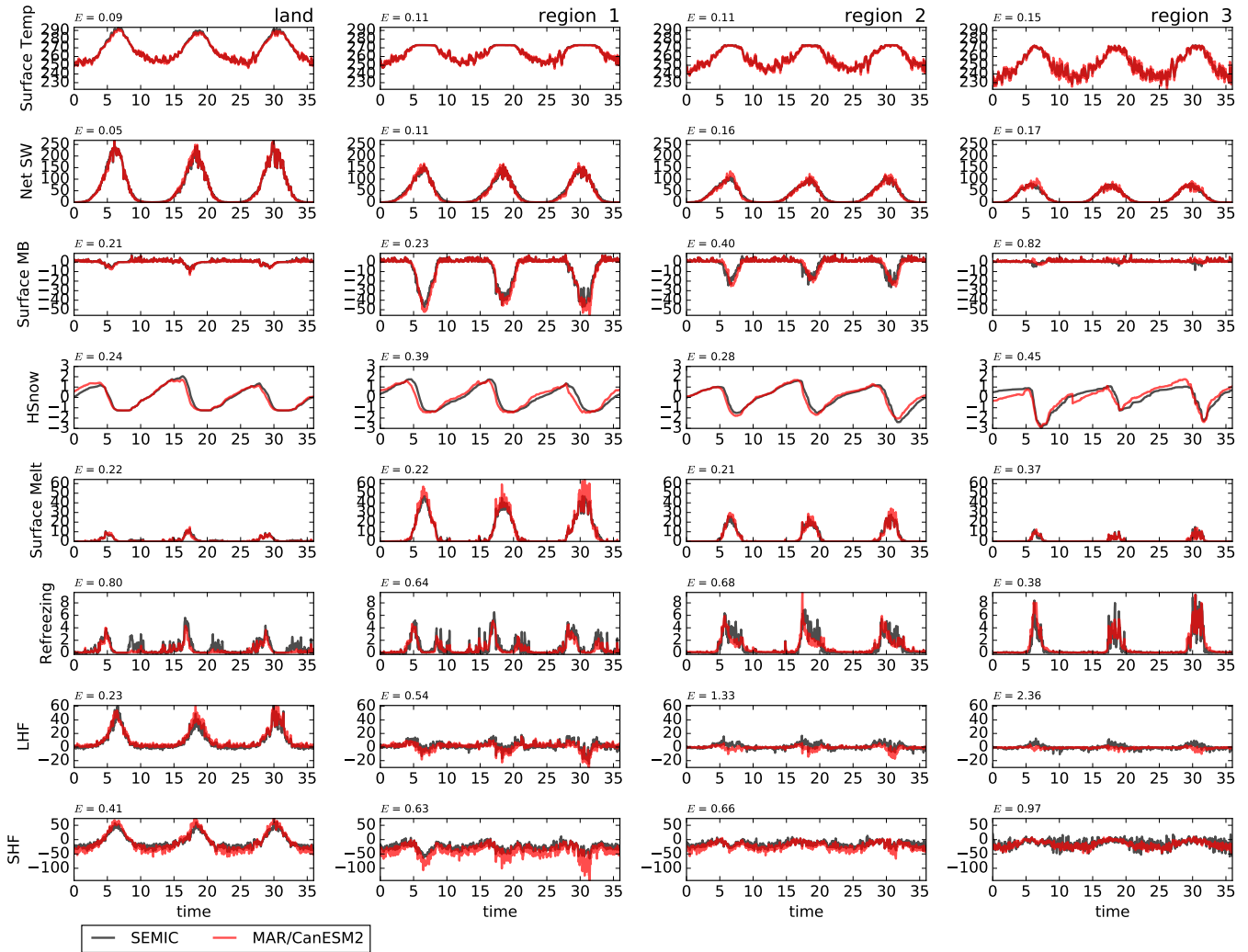


**Figure 5.** Time series of ice-sheet averaged surface temperature (in K), net shortwave radiation (in  $\text{W/m}^2$ ), surface mass balance (in mm/day), snow height (standardised by  $\sigma$ ), surface melt (in mm/day), refreezing (in mm/day), latent heat flux (in  $\text{W/m}^2$ ), and sensible heat flux (in  $\text{W/m}^2$ ) as calculated by MAR and by SEMIC with optimal parameters from Table 1 for the years 2098–2100 (= 36 months) of RCP8.5. Note that  $h_s$  is scaled via its standard deviation because SEMIC and MAR incorporate a different criterion of maximum snow height (5 m in SEMIC; more than 10 m in MAR). The annotated number on the top left of each frame is the computed centered root mean square error as defined in Eq. (20) and it marks the distance to the reference field as shown in the Taylor diagram Fig. 7.

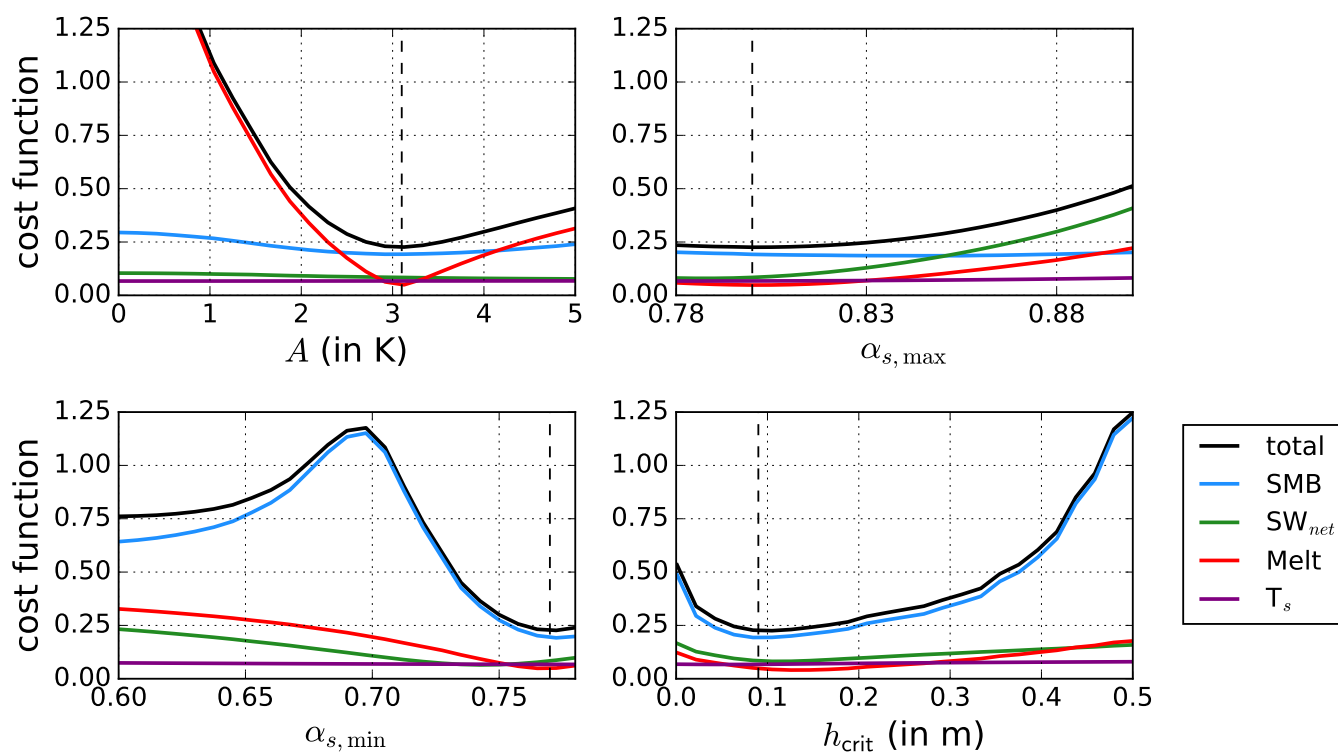


**Figure 6.** Sensitivity of cost function  $J$  for each of the free model parameters listed in Table 1, except  $\alpha_l$ . Solid black lines show the total cost function, i.e., the root mean square of the individual cost functions. Blue indicates the cost function of the surface mass balance, green the cost function of the net shortwave radiation, red the cost function of melt, and purple indicates the cost function of the surface temperature. The dashed lines in each plot indicate the optima as obtained by the particle swarm optimisation.

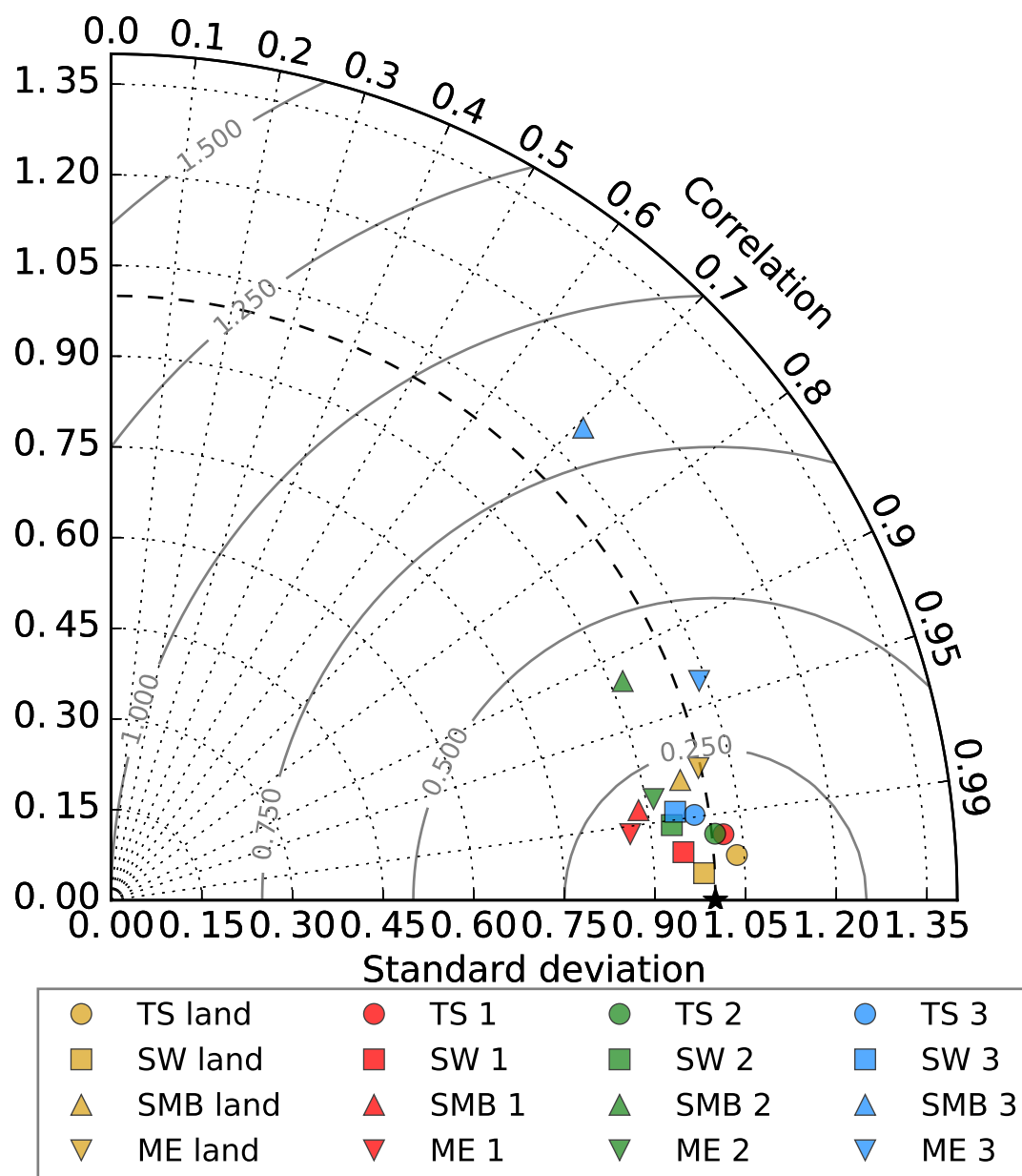


**Figure 7.** Taylor diagram of normalised surface temperature (TS), net shortwave radiation (SW), surface mass balance (SMB), and surface melt (ME) averaged over the whole Greenland ice sheet (as in Fig. 5). The black star denotes the reference field, which has (per definition) a standard deviation and a correlation coefficient of 1.

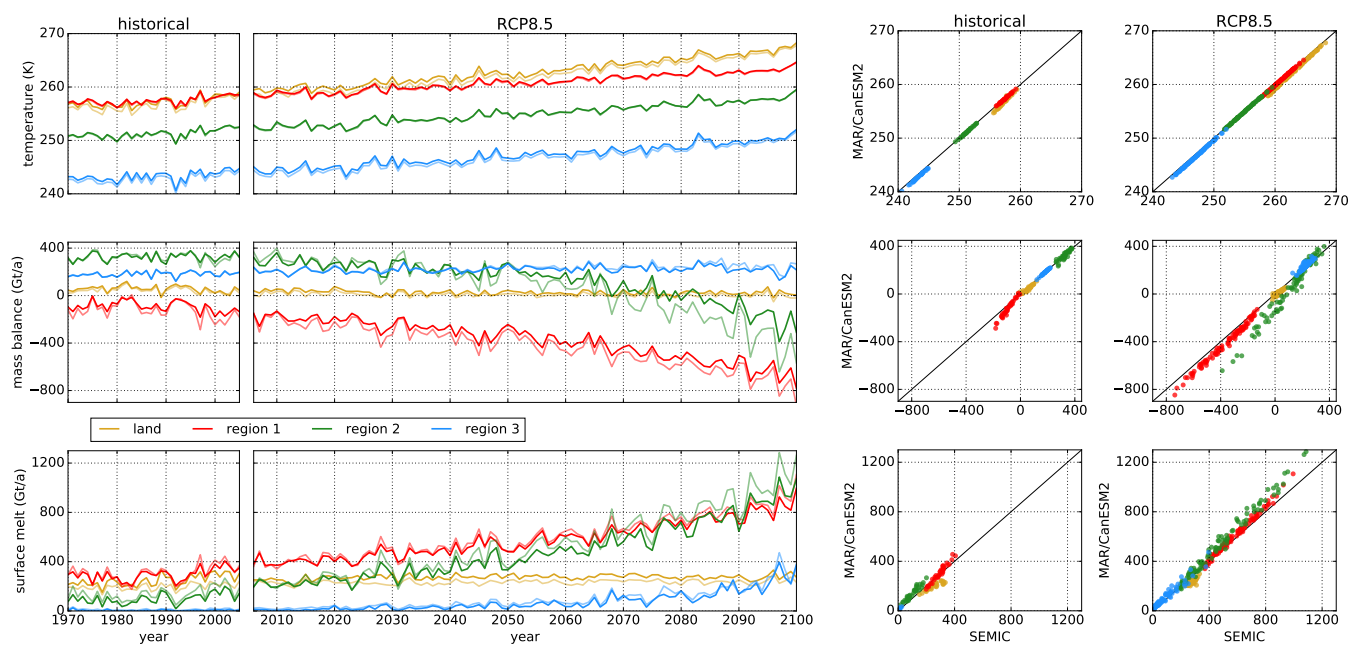


**Figure 8.** Left: Annual-mean, region-averaged surface temperature, surface mass balance, and surface melt for SEMIC (thick lines) and MAR (thin lines) using the optimal parameter values from Table 1. Right: Point-to-point comparison of the two models; variables and units as in the left panel.



## References

- Calov, R., Ganopolski, A., Claussen, M., Petoukhov, V., and Greve, R.: Transient simulation of the last glacial inception. Part I: glacial inception as a bifurcation in the climate system, *Climate Dynamics*, 24, 545–561, doi:10.1007/s00382-005-0007-6, 2005.
- Cuffey, K. and Paterson, W. S. B.: *The Physics of Glaciers*, Elsevier, 4th edn., 2010.
- 5 Fettweis, X., Franco, B., Tedesco, M., van Angelen, J. H., Lenaerts, J. T. M., van den Broeke, M. R., and Gallée, H.: Estimating the Greenland ice sheet surface mass balance contribution to future sea level rise using the regional atmospheric climate model MAR, *The Cryosphere*, 7, 469–489, doi:10.5194/tc-7-469-2013, 2013.
- Fitzgerald, P. W., Bamber, J. L., Ridley, J. K., and Rougier, J. C.: Exploration of parametric uncertainty in a surface mass balance model applied to the Greenland ice sheet, *Journal of Geophysical Research*, 117, F01 021, doi:10.1029/2011JF002067, 2012.
- 10 Gill, A. E.: *Atmosphere–Ocean Dynamics*, vol. 30 of *International Geophysics Series*, Academic Press, New York, 1982.
- Hanna, E., Navarro, F. J., Pattyn, F., Domingues, C. M., Fettweis, X., Ivins, E. R., Nicholls, R. J., Ritz, C., Smith, B., Tulaczyk, S., Whitehouse, P. L., and Zwally, H. J.: Ice-sheet mass balance and climate change, *Nature*, 498, 51–59, doi:10.1038/nature12238, 2013.
- Heinemann, M., Timmermann, A., Elison Timm, O., Saito, F., and Abe-Ouchi, A.: Deglacial ice sheet meltdown: orbital pacemaking and CO<sub>2</sub> effects, *Clim. Past*, 10, 1567–1579, doi:10.5194/cp-10-1567-2014, 2014.
- 15 Moss, R. H., Edmonds, J. A., Hibbard, K. A., Manning, M. R., Rose, S. K., van Vuuren, D. P., Carter, T. R., Emori, S., Kainuma, M., Kram, T., Meehl, G. A., Mitchell, J. F. B., Nakicenovic, N., Riahi, K., Smith, S. J., Stouffer, R. J., Thomson, A. M., Weyant, J. P., and Wilbanks, T. J.: The next generation of scenarios for climate change research and assessment, *Nature*, 463, 747–756, doi:10.1038/nature08823, 2010.
- Nghiem, S. V., Hall, D. K., Mote, T. L., Tedesco, M., Albert, M. R., Keegan, K., Shuman, C. A., DiGirolamo, N. E., and Neumann, G.: The extreme melt across the Greenland ice sheet in 2012, *Geophysical Research Letters*, 39, L20 502, doi:10.1029/2012GL053611, 2012.
- 20 Ohmura, A.: Physical Basis for the Temperature-Based Melt-Index Method, *Journal of Applied Meteorology*, 40, 753–761, doi:10.1175/1520-0450(2001)040<0753:PBFTTB>2.0.CO;2, 2001.
- Poli, R., Kennedy, J., and Blackwell, T.: Particle swarm optimization, *Swarm Intelligence*, 1, 33–57, doi:10.1007/s11721-007-0002-0, 2007.
- Reeh, N.: Parameterization of melt rate and surface temperature on the Greenland ice sheet, *Polarforschung*, 59, 113–128, 1991.
- Reijmer, C. H., van den Broeke, M. R., Fettweis, X., Ettema, J., and Stap, L. B.: Refreezing on the Greenland ice sheet: a comparison of parameterizations, *The Cryosphere*, 6, 743–762, doi:10.5194/tc-6-743-2012, 2012.
- 25 Robinson, A. and Goelzer, H.: The importance of insolation changes for paleo ice sheet modeling, *The Cryosphere*, 8, 1419–1428, doi:10.5194/tc-8-1419-2014, 2014.
- Robinson, A., Calov, R., and Ganopolski, A.: An efficient regional energy-moisture balance model for simulation of the Greenland Ice Sheet response to climate change, *The Cryosphere*, 4, 129–144, doi:10.5194/tc-4-129-2010, 2010.
- 30 Slater, A., Pitman, A., and Desborough, C.: The validation of a snow parameterization designed for use in general circulation models, *International Journal of Climatology*, 18, 595–617, doi:10.1002/(SICI)1097-0088(199805)18:6<595::AID-JOC275>3.0.CO;2-O, 1998.
- Taylor, K. E.: Summarizing multiple aspects of model performance in a single diagram, *Journal of Geophysical Research: Atmospheres*, 106, 7183–7192, doi:10.1029/2000JD900719, 2001.
- Thomas, R., Frederick, E., Li, J., Krabill, W., Manizade, S., Paden, J., Sonntag, J., Swift, R., and Yungel, J.: Accelerating ice loss from the fastest Greenland and Antarctic glaciers, *Geophysical Research Letters*, 38, L10 502, doi:10.1029/2011GL047304, 2011.
- van de Berg, W., van den Broeke, M., Ettema, J., van Meijgaard, E., and Kaspar, F.: Significant contribution of insolation to Eemian melting of the Greenland ice sheet, *Nature Geoscience*, 4, 679–683, doi:10.1038/ngeo1245, 2011.



van den Broeke, M., Bamber, J., Ettema, J., Rignot, E., Schrama, E., van de Berg, W., van Meijgaard, E., Velicogna, I., and Wouters, B.:

Partitioning Recent Greenland Mass Loss, *Science*, 326, 984–986, doi:10.1126/science.1178176, 2009.

Vionnet, V., Brun, E., Morin, S., Boone, A., Faroux, S., Le Moigne, P., Martin, E., and Willemet, J.-M.: The detailed snowpack scheme

Crocus and its implementation in SURFEX v7.2, *Geoscientific Model Development*, 5, 773–791, doi:10.5194/gmd-5-773-2012, 2012.